Focal Mechanism Determinations of the 1991 Chiali Earthquake (M_L=5.7) Sequence

Kuo-Fong Ma[1] and Jung-Yu Chen[1,2]

ABSTRACT

The focal mechanisms of the 1991 Chiali earthquake sequence were investigated by considering the first motion data and available strong motion waveforms. Due to the sparse distribution of the first-motion data, the first-motion solutions are multiple for the earthquake sequence. By considering the waveform mechanism, which is determined by considering the amplitude ratio of P, SV and SH waveform, as the constraint, we chose the optimum first-motion mechanisms of the earthquake sequence. Either the optimum first-motion mechanisms or the waveform mechanisms of most of the aftershocks show thrust faulting mechanism. Except for the event E-3, the waveform mechanisms of the earthquake sequence have a northeast-southwest striking plane similar to the distribution of aftershock sequence, while the optimum first-motion mechanisms of the earthquake sequence show more complex focal mechanisms. Compared with the aftershock distribution in consideration of the waveform mechanisms of the earthquakes, the fault plane with NE-SW strike and NW dipping plane is suspected as the preferred fault plane. Since the location of the earthquake is near the transition between the extension mechanism of southwestern Asian passive margin and the compression mechanism due to Luzon arc collision, the thrust faulting mechanism of the Chiali earthquake might indicate an ongoing compression mechanism due to arc-continental collision in such an extensional environment. The b value of about 0.7 in this region implies a relatively stable tectonic environment compared with other regions in Taiwan. The larger ratio of the logarithm of cumulative seismic moment of aftershocks to that of the seismic moment of the mainshock for the 1991 Chiali earthquake (about 1) also suggests a smaller stress drop for this earthquake is compared with other moderate size earthquakes in the Chianan region.

(Key words: Chiali earthquake, Focal mechanism, Seismic moment)

---

[1]Institute of Geophysics, National Central University, Taiwan, ROC
[2]Seismological Observation Center, Central Weather Bureau, Taiwan, ROC

1. INTRODUCTION

The 1991 Chiali earthquake (M_L=5.7), at the latitude of 23.25° and longitude of 120.08°, occurred on 12 March 1991, at a depth of 12.26 km off the coast of southwestern Taiwan (Central Weather Bureau Seismological Network Report). No earthquake with M>5.5 had been recorded since 1973 in this area (latitude of 22.9°~23.5°; longitude of 119.6°~120.3°). Since this region had long been considered a region of high seismic hazard potential, the Chiali earthquake attracted attention to the seismic activity in that region.

The mechanisms of regional earthquakes are traditionally determined from P-wave first-motion data. The initial motions are usually very sparse for small events and, thus, it is difficult to determine the fault plane solution, especially for offshore events. The seismic network operated by the Institute of Earth Science, Academia Sinica and National Chung-Cheng University recorded complete waveforms, not only for the mainshock but also for some of the aftershocks. Since some of the stations are close to the epicenters of the earthquakes, these records are relatively free from contamination by propagation path effect. These waveforms can be used as a constraint on the determination of focal mechanisms. A combined use of the waveforms and first-motion data enables us to obtain the overall mechanism that explains the first-motion and waveform data.

The focal mechanism of the mainshock using P-wave first motions is the strike slip mechanism (Shin et al., 1993). Thus, it is concluded that this earthquake is probably associated with the Tsengwen-Hsi fault. However, the focal mechanisms of the aftershocks determined by Hsu and Ho (1993) from first-motion data, show most of the thrust faulting mechanisms. Although the mechanisms of the aftershocks are not necessarily consistent with those of the mainshock, the discrepancy between the mechanisms of the mainshock and aftershocks might affect the interpretation of the results. With the additional waveform data mentioned above, we try to investigate the mechanisms of the earthquake sequence with M>4 using waveforms and first-motion data to understand the characteristics of the earthquake. We considered the first motions as the basis and the waveform information of each event as the constraint to obtain the optimum first-motion focal mechanism and the waveform mechanism. Since it is difficult to judge whether either the optimum first-motion mechanism or the waveform mechanism is the representative focal mechanism, we considered the both focal mechanisms as possible focal mechanisms of the earthquake.

2. DATA

One hundred and eighty aftershocks were recorded by the Central Weather Bureau Seismographical Network (CWBSN) during the period from the 12 March 1991 to 12 April 1991 in the area shown in Figure 1. Of these, 18 events are with magnitude 4.0 or larger. The seismographic network, which was composed of 14 stations with SSR and FBA-23 accelergraphy (Figure 1), operated by the National Chung Cheng University, recorded nice waveforms for some of the events. In addition, three portable instruments were deployed by the Institute of Earth Science, Academia Sinica, at BAI, CHI and LON stations right after the

03120604 aftershock and station distribution
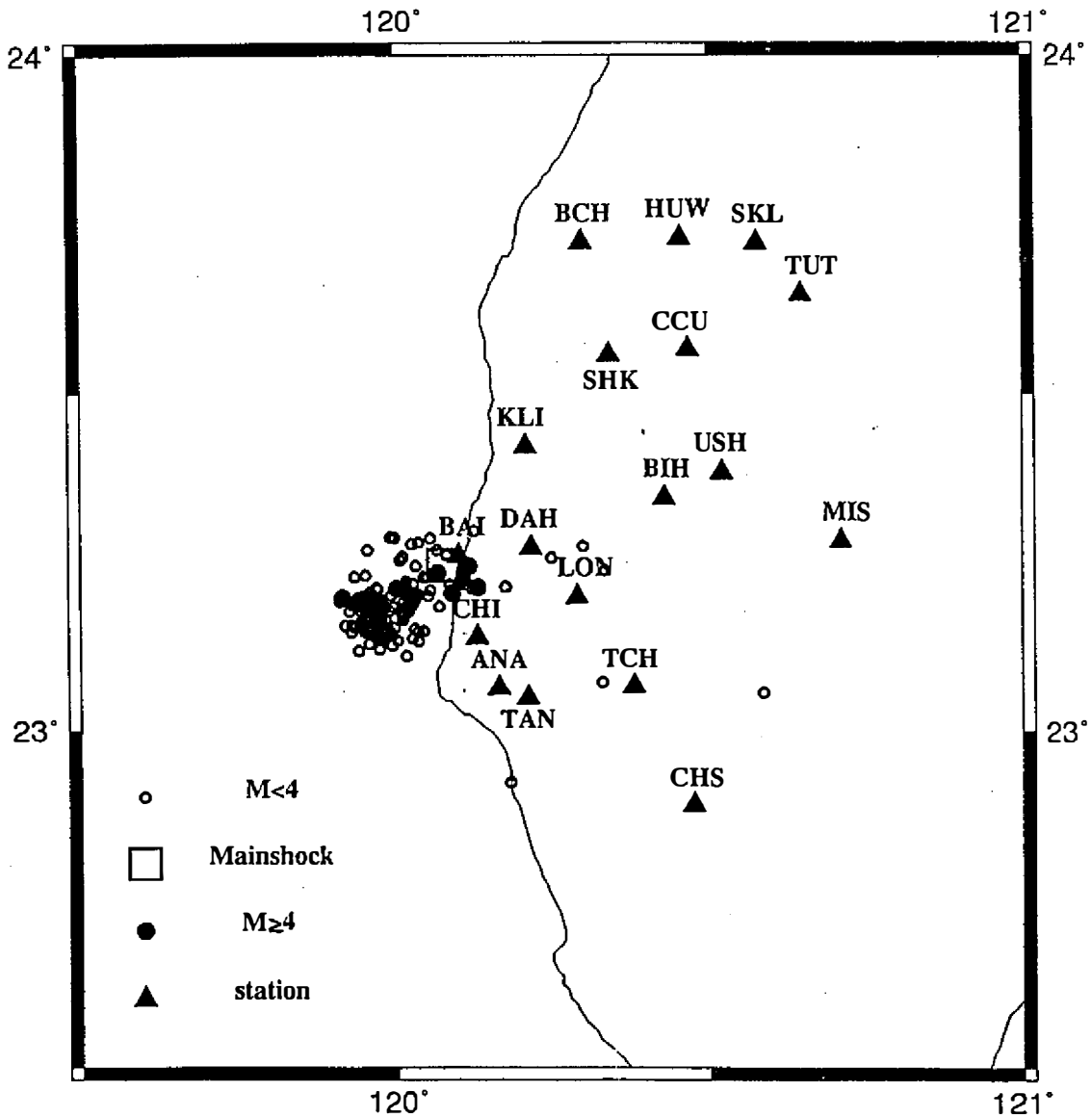
Fig. 1. Distribution of the 1991 Chiali earthquake sequence. The open and solid circles represent the earthquakes with magnitude less than 4.0 and equal or larger than 4.0, respectively. Square symbols indicate the location of mainshocks. The solid triangles represent the distribution of strong motion stations operated by Institute of Earth Science, Academia Sinica, and Institute of Seismology, National Chung-Cheng university.

earthquake (Figure 1). These portable instruments were very close to the epicenters of the earthquake sequence and provided important information of the earthquakes. We rotated the acceleration records into the transverse and radial components, and integrated them twice to obtain ground-motion displacement records. In this study, we investigate only the events which were recorded by two stations with clear P, SV and SH waveforms. After examination, we focused on seven events including the mainshock in our investigation as listed in Table 1. The stations used in this study for each event are listed in Table 2. Table 2 also lists the epicentral distances of the station for the corresponding events. Figure 2a~2g show the corresponding displacement waveforms of the selected stations for the earthquake sequence. Since the chosen stations of each event are close to the epicenter, the path effect is negligible; except for the SV at vertical component, they show clear displacement waveforms of direct P, SV at radial component and SH, which were used to determine the focal mechanisms of the earthquakes. The small SV at vertical component is due to the low velocity layer near the surface in this region. Hence, this study only considers the amplitude ratios and polarities of P at vertical component, SV at radial component and SH at transverse component.

Other waveforms are not used in this study because of unclear P, SV and SH due to the path effect or site effect. Events for which nice waveforms were recorded by two or more stations are used to determine the focal mechanism. The waveform mechanism is used as the constraint to compare with the focal mechanism determined by first-motion data.

The polarities of the first motions of the earthquake sequence were re-examined from the short period waveforms of the Central Weather Bureau Seismographic Network (CWBSN). The azimuth and take-off angles of each station were computed using the velocity model determined by Ho (1994) for the southwestern region.

3. METHOD

The first motion mechanism of each event was determined by using program FPFIT (Reasenberg and Oppenheimer, 1985), which is conducted through a two-stage grid-search procedure that finds the best solution minimizing a normalized, weighted sum of first-motion polarity discrepancies. In addition to finding the minimum-misfit solution, FPFIT finds alter-

Table 1. The origin times, locations, and magnitudes of the mainshock and aftershocks of Chiali (M5.7) earthquake sequence used in this study. The event number is assigned as listed in the Table.

Event Number	Date (m/d/yr)	Origin time	Lat. (°N)		Long. (°W)		Depth (km)	M_L
E-0	3/12/1991	06:04:06.14	23	14.74	120	04.47	12.26	5.7
E-1	3/12/1991	06:54:24.72	23	13.36	120	06.35	7.44	4.9
E-2	3/14/1991	04:27:43.82	23	09.06	119	57.19	6.61	4.3
E-3	3/15/1991	07:56:40.41	23	09.79	119	58.22	12.15	4.4
E-4	3/15/1991	15:06:32.73	23	08.99	119	58.33	12.10	4.8
E-5	3/17/1991	04:37:05.74	23	10.72	120	00.66	9.68	5.2
E-6	3/22/1991	06:08:53.55	23	12.79	120	00.71	13.32	4.6

native solutions corresponding to significant relative minima in misfit.

Upper panels of the Figure 3a~3g show the possible first motion mechanisms of each event for the earthquake sequence. Most of the events have multiple first motion mechanisms determined by FPFIT due to the sparse distribution of the first motions.

The method for the waveform mechanism determination used in this study is essentially the same as that used by Ma and Kanamori (1991). The P, SV, and SH far-field displacements, U_r, U_θ, and U_ϕ, from a double-couple point source are given by

$$
\begin{bmatrix} U_r \\ U_\theta \\ U_\phi \end{bmatrix} = \frac{M_o s(t)}{4\pi\rho r\alpha^3} \begin{bmatrix} R^p \\ (\alpha/\beta^3)R^{SV} \\ (\alpha/\beta^3)R^{SH} \end{bmatrix} \tag{1}
$$

where s(t) and M_o are the unit moment rate function and the seismic moment, respectively. Here, ρ, α, and β are density, P velocity, and S velocity, which are 2.6 g/cm^3, 6 km/sec, and 3.5 km/sec, respectively. R^P, R^{SV}, and R^{SH} are P-wave, SV-wave and SH-wave radiation patterns respectively. The radiation patterns are functions of the fault parameters: dip δ, rake λ, and strike ϕ. We use (1) to determine M_o, δ, λ, and ϕ from U_r, U_θ, and U_ϕ estimated from the observed P, SV, and SH amplitudes and polarities.

Let U_P, U_{SVZ}, U_{SVR}, and U_{SH} be the displacements of P wave on the vertical component, the SV wave on the vertical component, the SV wave on the radial component, and the SH wave on the tangential component, respectively, observed at the free surface, then

Table 2. The epicentral distances and incident angles of the used stations for the corresponding events.

event number	stations	epicentral distance (km)	incident angle (deg.)
E-0	KLI	23.6	36.3
	BCH	57.8	35.3
E-1	KLI	24.2	43.2
	SHK	44.1	37.8
E-2	CHI	18.2	43.0
	BAI	19.3	43.2
E-3	CHI	16.6	33.9
	BAI	17.1	34.2
E-4	KLI	38.4	35.3
	BAI	17.9	34.7
E-5	KLI	33.4	37.8
	BAI	12.8	35.5
E-6	KLI	30.4	35.3
	BAI	10.4	25.6
	CHI	14.5	30.6
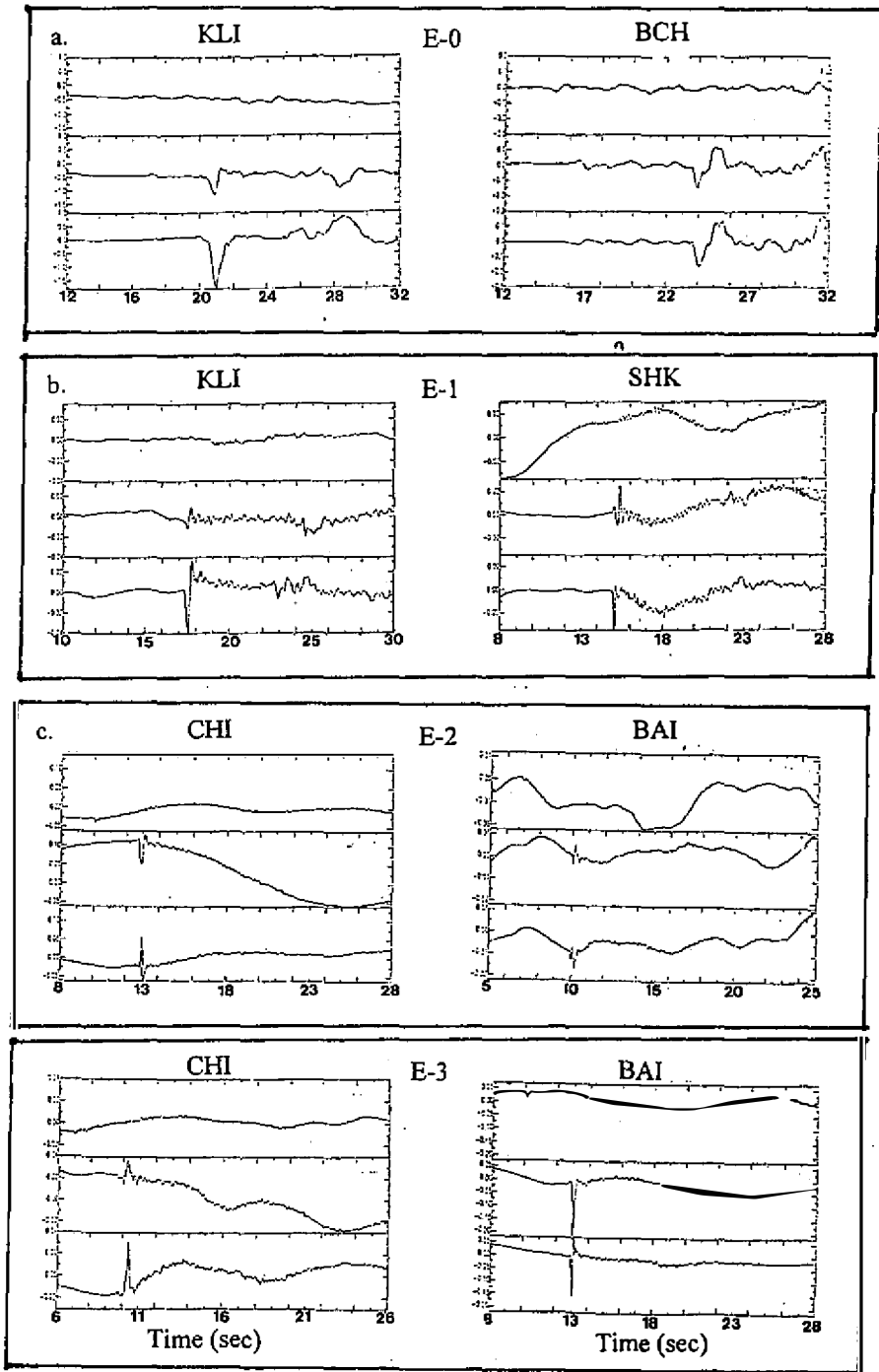
Fig. 2. Integrated displacement waveforms at the available stations for events
(A) E-0 to (G) E-6.

e.

KLI   E-4   BAI

f.

KLI   E-5   BAI

g.

KLI   E-6   BAI

Time (sec)

CHI

Time (sec)
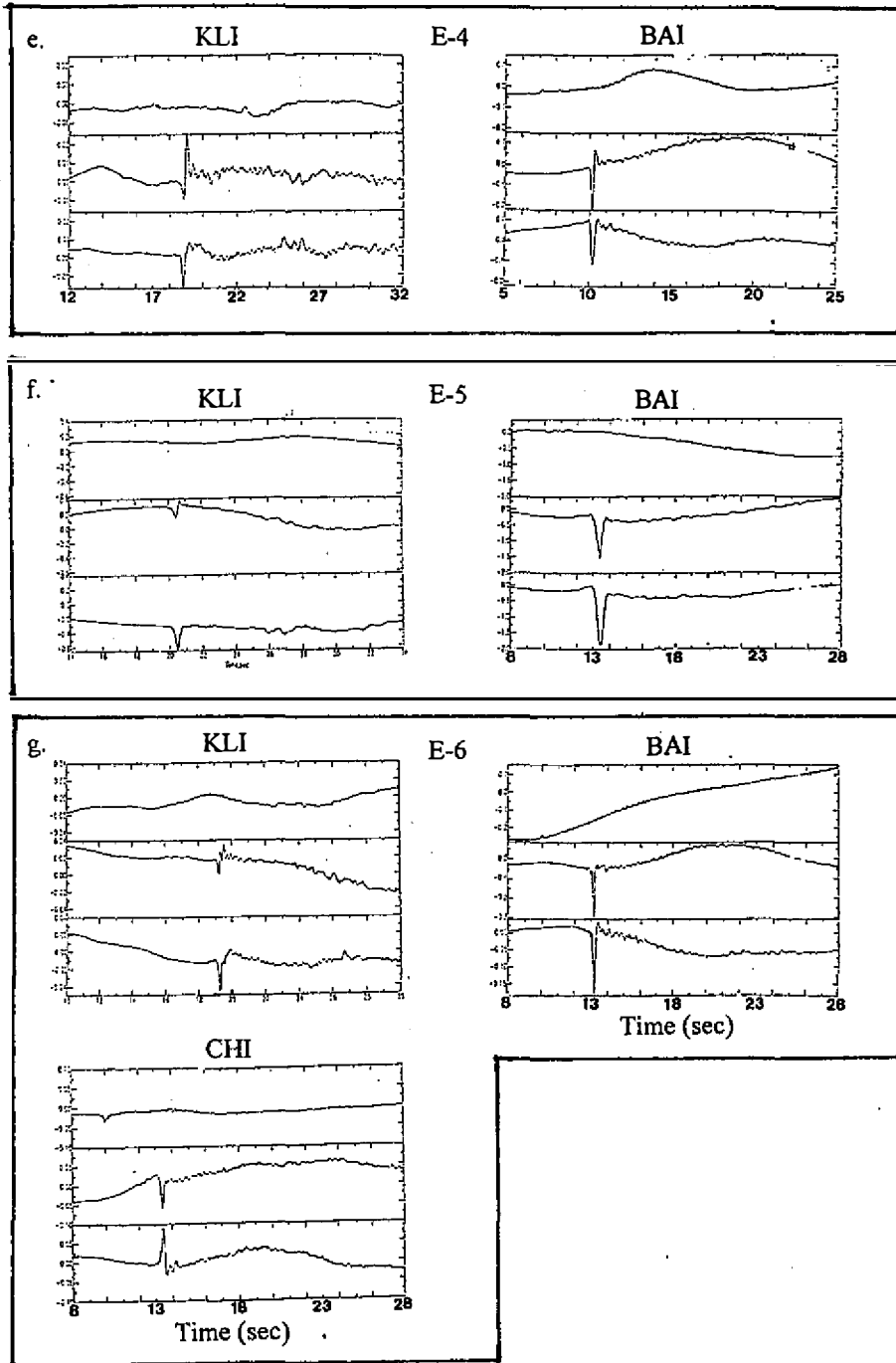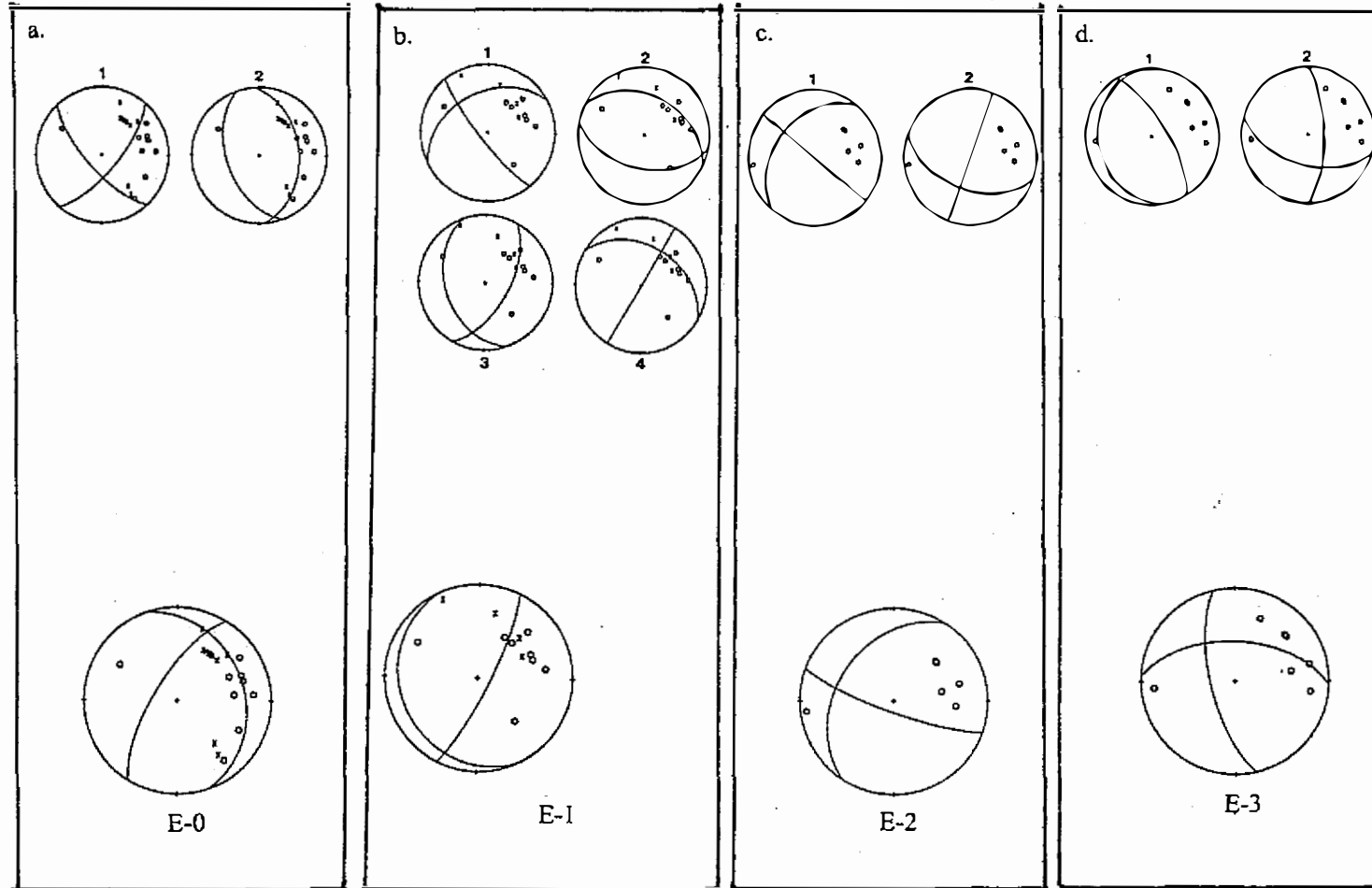
(*Fig. 2.* continued)

Fig. 3. Possible first motion mechanisms through FPFIT (top), and available waveform mechanism (bottom) for events (a) E-0 to (g) E-6. Open and cross symbols represent the dilatation and compression of first motions.
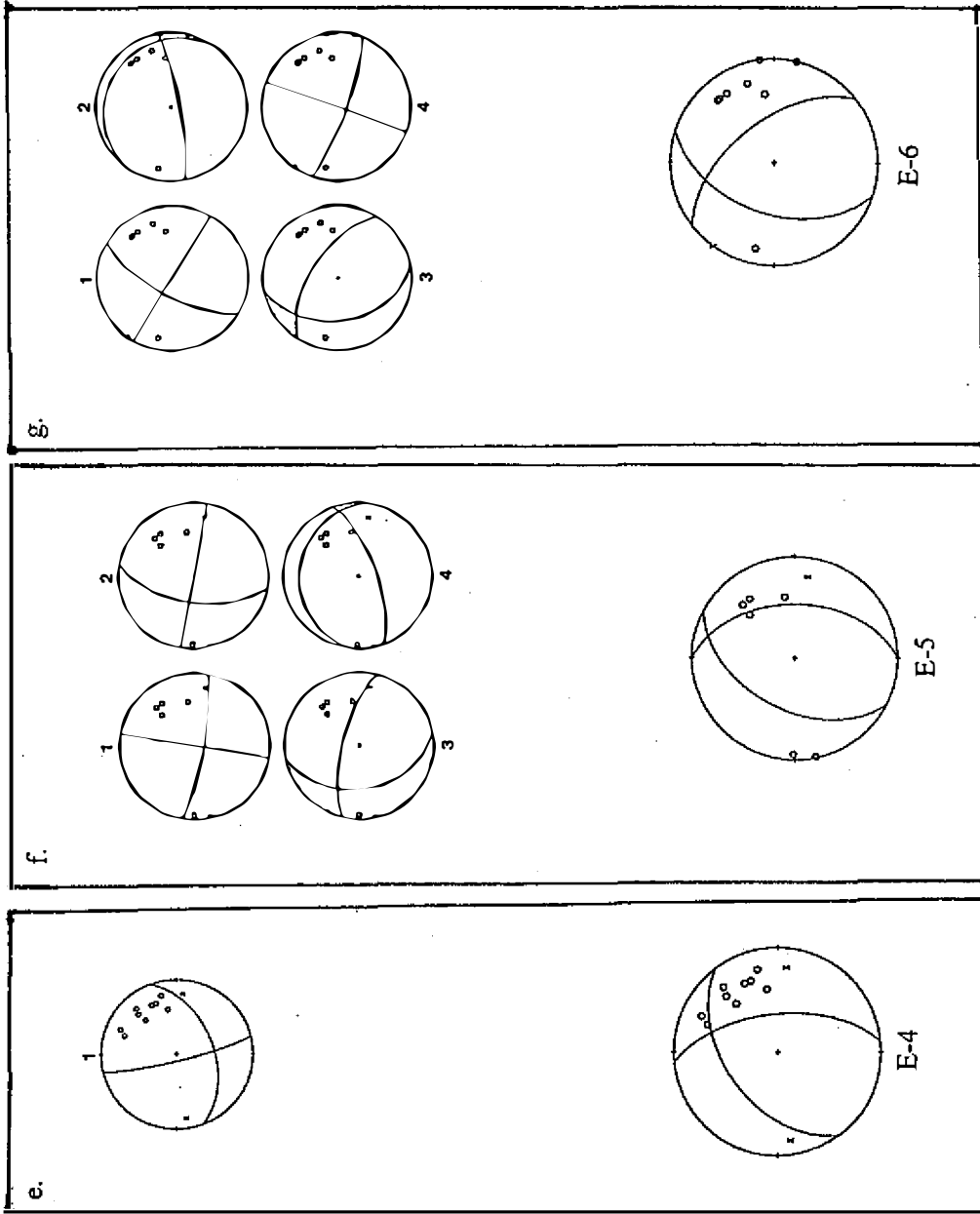
(*Fig. 3.* continued)

$$U_r = U_P/(2\cos i_o)$$
$$U_\theta = U_{SVZ}/(-2\sin i_o) = U_{SVR}/(2\cos i_o) \qquad\qquad (2)$$
$$U_\phi = U_{SH}/2,$$

where i_o is the incident angle. The free-surface effect is approximated by a factor of 2 of amplification of the incidence wave. Within the critical angle, the factor of 2 of the free-surface approximation is satisfactory. Due to the affect of the low velocity layer near the free surface, the SV waveform at the vertical component is hardly visible as shown in Figure 2a~2g. In this study, we measured the SV wave at radial component. The amplitude of SV wave, U_θ, used in equation (1) was, then, corrected by considering the incident angle as stated in Equation (2). The incident angle was calculated using Ho's (1994) southwestern velocity model, with a low velocity layer near the surface. Table 2 also lists the incident angles of the stations for the corresponding events.

In this study, we only use stations that are close to the epicenter, so the propagation effect data are simple and the free-surface approximation mentioned above is satisfactory. For the events whose waveform data were from more than one station, the solution of (1) could be obtained by using general least-square method. The bottom panels of Figures 3a~3g show the waveform mechanisms thus determined.

For each event, the P and T axes of the first-motion mechanisms and the waveform mechanism are compared. Among them, we chose an optimum first-motion mechanism whose locations on the P and T axes are the most similar to that of the waveform mechanism. The synthetics of P, SV and SH waveforms of both the optimum first-motion mechanism and the waveform mechanism are produced to see the compatibility of the waveforms to the observed. Since it is difficult to judge whether the first-motion data or the observed waveform is more reliable, in this study, we considered that both the optimum first-motion mechanism and waveform mechanism were the possible mechanisms of the earthquake sequence.

4. RESULTS

There are two first motion mechanisms for the mainshock, E-0 (Figure 3a). One indicates the strike-slip focal mechanism, the other indicates thrust faulting focal mechanism. The waveform focal mechanism determined from stations KLI and BCH also exhibits the thrust faulting mechanism (Figure 3a). Although station BCH has an epicentral distance of over 50 km, the waveforms shown in Figure 2a still exhibit clear P, SV and SH waveforms, which are good for our analysis. From comparing the first motion mechanisms and waveform mechanism of the locations of P and T axes, we identified the thrusting mechanism of the first motion mechanism as the optimum first-motion mechanism. The amplitude ratio and polarities of the synthetics of P, SV at radial component and SH for the first motion mechanism are quite comparable with the observation shown in Figure 4a for station KLI. However, the SV at radial component of the synthetics for station BCH also shown in Figure 4a, does not show polarity comparable with the observation. Figure 5a shows the synthetics for the waveform mechanism

for stations KLI and BCH. They both produce waveforms comparable to the observation.

Figure 3b shows the first motion mechanism and waveform mechanism for event E-1. Due to the random distribution in the first-motion data, it shows four first-motion mechanisms after FPFIT. They have very different focal mechanisms (Figure 3b). The waveform mechanism derived from stations SHK and KLI shows a thrust focal mechanism. For the small events, the displacement records show a long term background noise, which causes nonzero baseline. In this study, we measured the amplitudes and polarities of the P, SV and SH by removing the effects of the nonzero baseline. From the comparison of the P and T axes of the waveform mechanism and first motion mechanisms, we chose the third first motion mechanism as the optimum solution. Figure 4b shows the synthetics of this solution for station KLI and SHK for the optimum first-motion mechanism. Except for the polarities of SV at radial components at station KLI and SHK, the synthetics are comparable with the observations. Figure 5b shows the synthetics of stations KLI and SHK for the waveform mechanism for comparison.

Two first motion mechanisms were obtained for the event E-2 (Figure 3c). One of them has a focal mechanism similar to the waveform mechanism derived from the stations CHI and BAI. This suggests the first first-motion mechanism is the optimum solution of the earthquake. The synthetics for this solution are also shown in Figures 4c and 5c for the optimum first-motion mechanism and waveform mechanism, respectively. They both produce similar amplitude ratios and polarities of P, SV at radial component and SH to the observation.

There are also two first-motion mechanisms for event E-3. The waveform mechanism was derived from the stations of CHI and BAI. From a comparison of the locations of P and T axes, we suggest the second first-motion mechanism as the preferred first-motion solution of the event. The synthetics are shown in Figure 4d and 5d for the first-motion mechanism and waveform mechanism, respectively. The synthetics of the first-motion mechanism produce not quite comparable amplitude ratios and polarities for the two stations, while, except for the SH wave at station BAI, the synthetics of the waveform mechanism are comparable with the observed.

There is only one first-motion mechanism for event E-4. It is very different from the waveform mechanism derived from stations KLI and BAI (Figure 3e). The synthetics shown in Figure 4e for the first-motion solution show different amplitude ratios and polarities from those observed at both stations KLI and BAI. Although the synthetics for the waveform mechanism shown in Figure 5e exhibit similar synthetics to the observations, there are some misfits of the first motions for the waveform mechanism. As mentioned above, it is still difficult to judge which solution is the most representative focal mechanism of the event. Thus, we still leave the two solutions as the possible focal mechanism of the event.

Figure 3f shows four first-motion mechanisms for event E-5. The third first-motion mechanism, among the first motion solutions, has the most similar locations of P and T axes to those of waveform mechanism. Figure 4f and 5f show the synthetics for the first-motion solution and waveform mechanism, respectively, for stations KLI and BAI. They both show synthetics comparable to the observed.

There are also four first-motion mechanisms for event E-6, as shown in Figure 3g. The third first-motion solution showing thrust-faulting mechanism is comparable with the waveform mechanism inverted from stations KLI, BAI and CHI. This first motion solution and
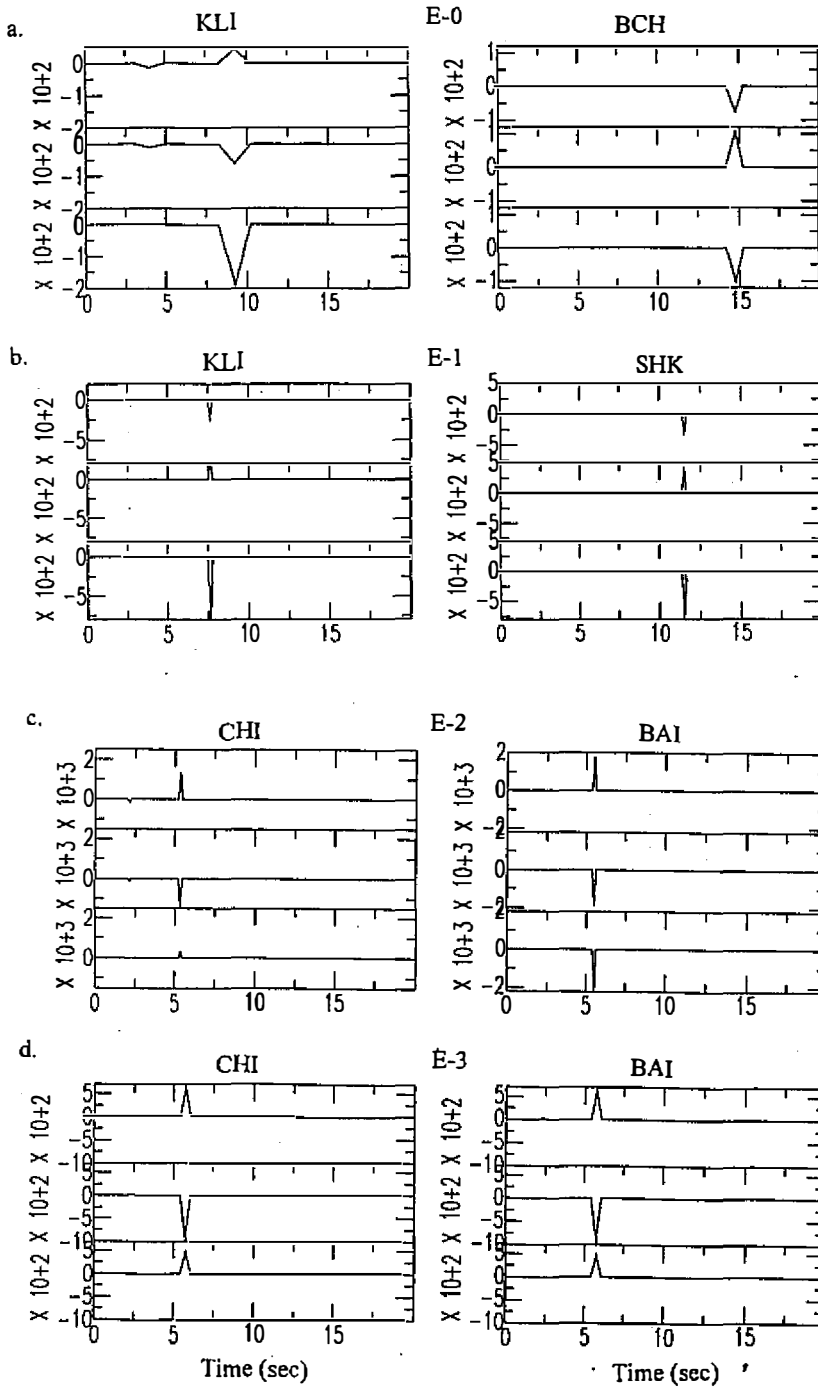
Fig. 4. Synthetics P, SV and SH waveforms for the optimum first-motion mecha-
nism for events (a) E-0 to (g) E-6.
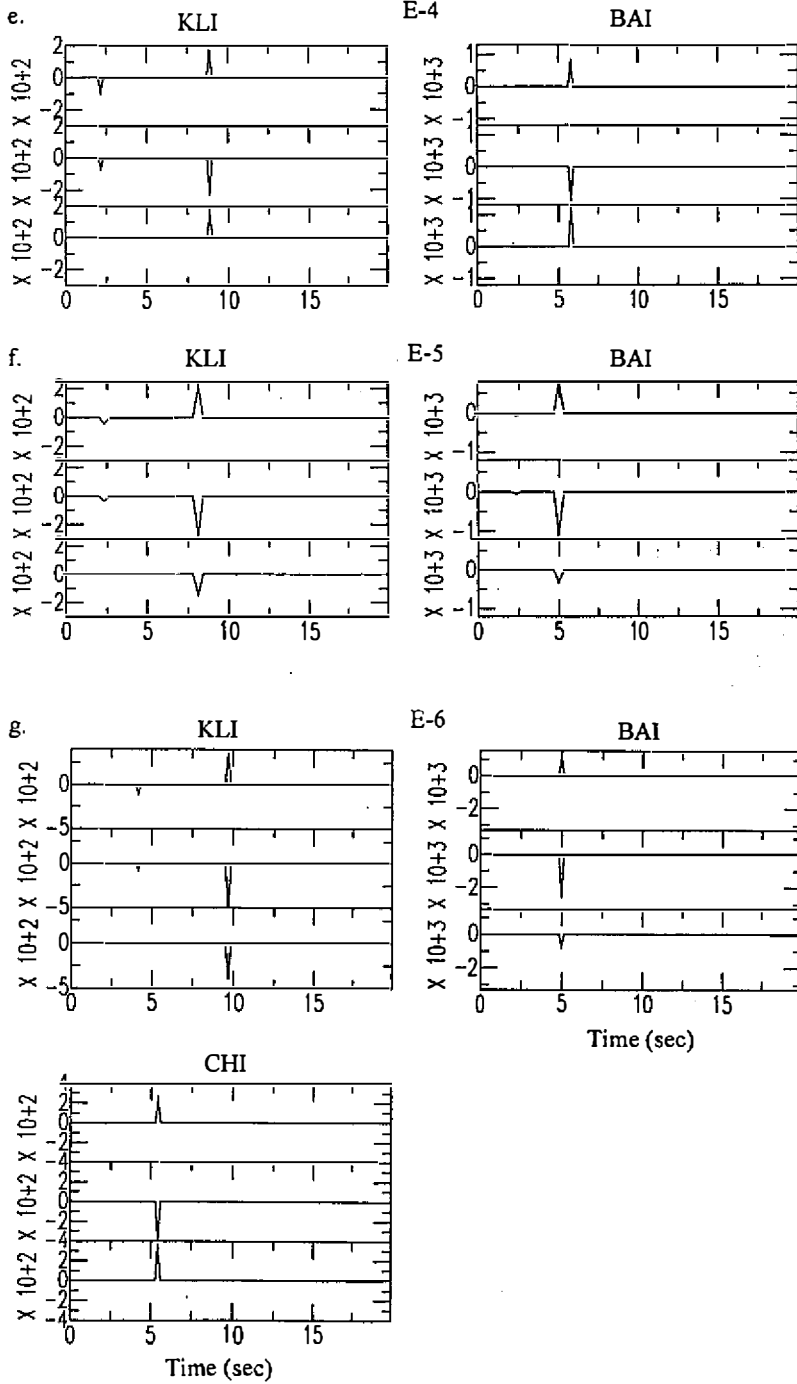
(*Fig. 4.* continued)
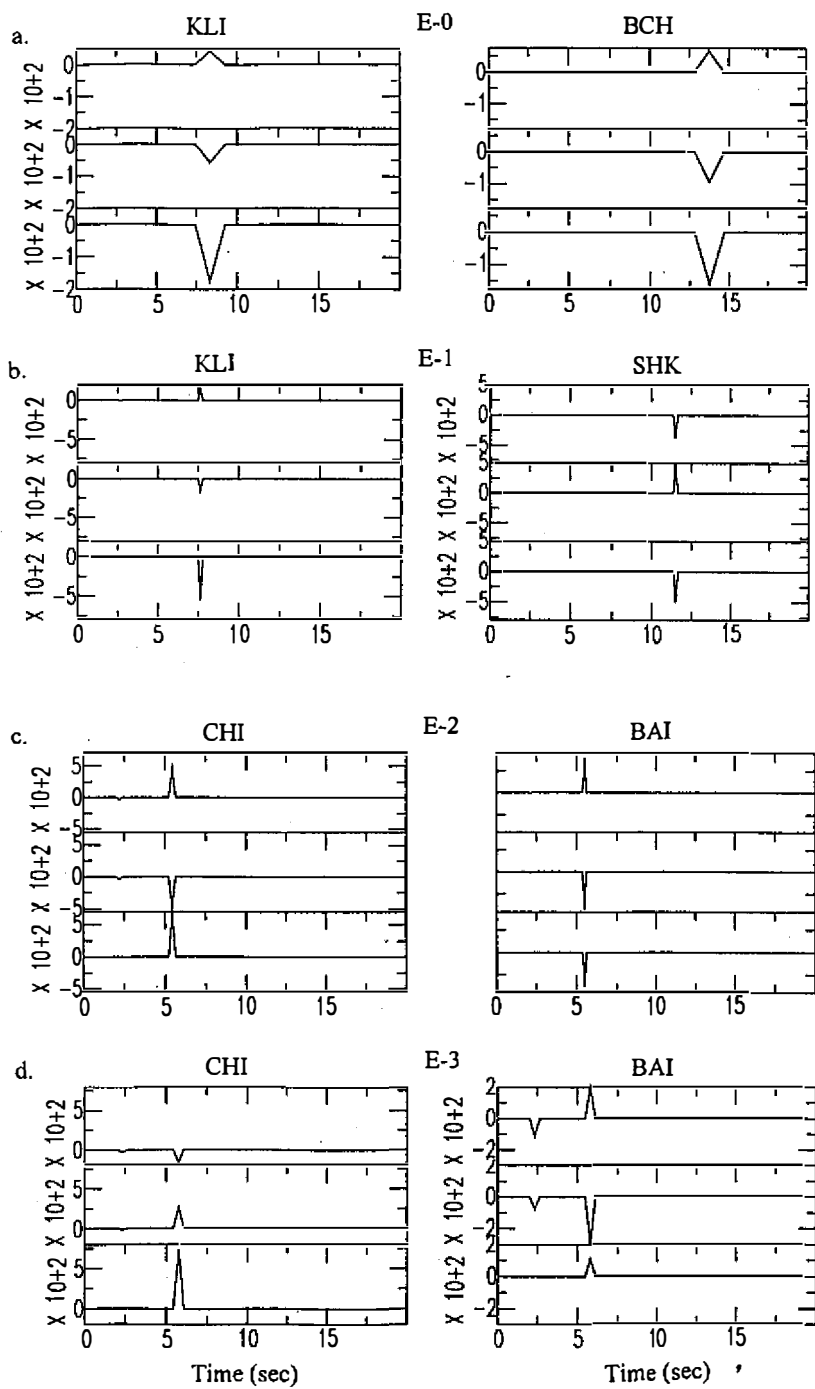
Fig. 5. Synthetics P, SV and SH waveforms for the waveform mechanism for events (a) E-0 to (g) E-6.
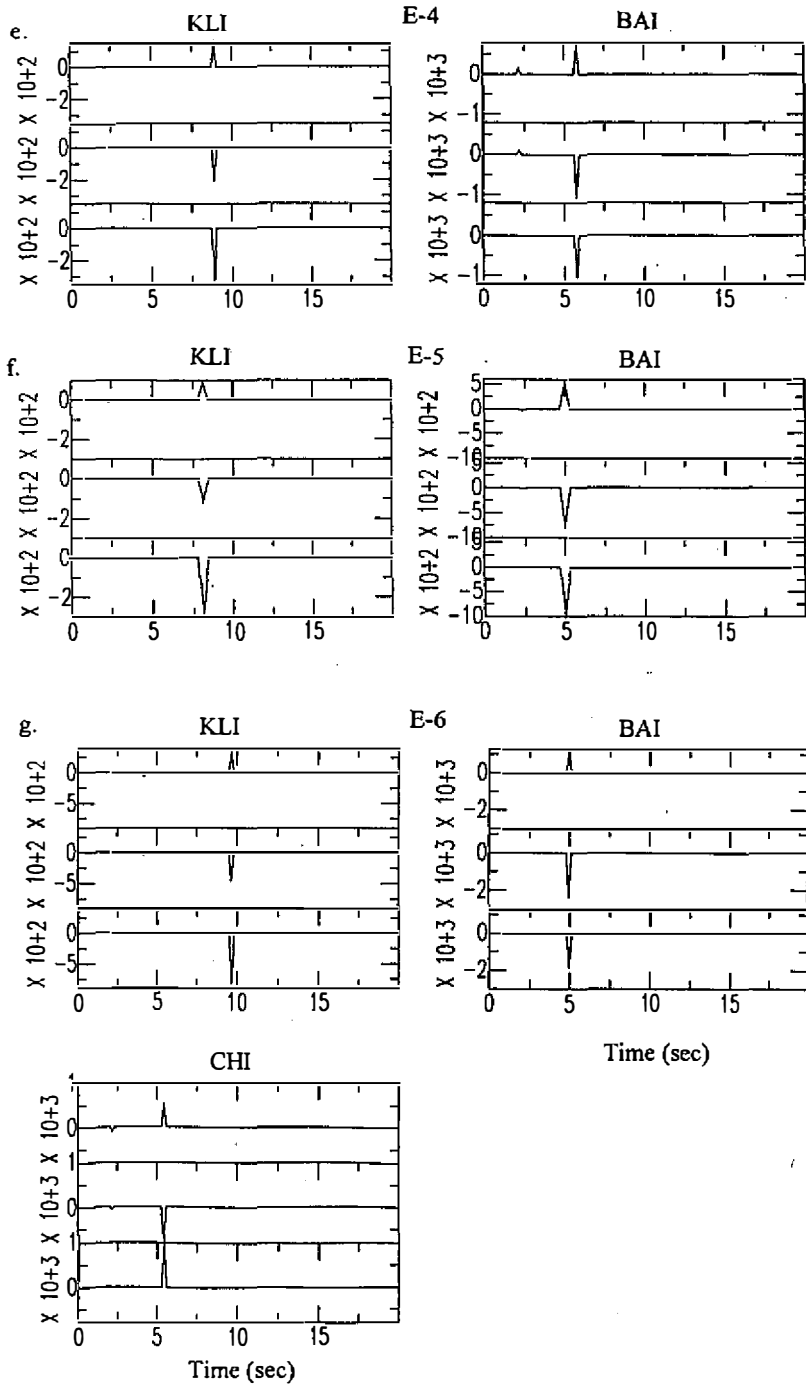
(*Fig. 5*. continued)

waveform mechanism also produce the waveforms comparable with the observations as shown in Figure 4g and 5g, respectively.

Table 3 lists the optimum first-motion mechanisms and waveform mechanisms thus determined for the earthquake sequence. Table 3 also lists the seismic moments of the earthquake sequence, estimated by using the pulse width and amplitude of the SH waveform.

5. DISCUSSION

Figures 6a and 6b show the spatial distribution of the mainshock and aftershocks of the Chiali earthquake sequence, with the optimum first-motion focal mechanisms and waveform mechanism, respectively, shown in equal-area projections of the lower focal hemisphere Most of the events are located to the southwest of the mainshock. Although there are some ambiguities in the determination of the focal mechanism, either optimum first-motion mechanisms or the waveform mechanisms of most of the aftershocks show thrust faulting mechanism. Except for event E-3, the waveform mechanisms of the earthquake sequence have a northeast-southwest striking plane similar to the distribution of aftershock sequence. The optimum first-motion mechanisms of the earthquake sequence show more complex focal mechanisms. Figures 7a and 7b show the projections of the P and T axes of the optimum first-motion mechanism and waveform mechanism, respectively, for the earthquake sequence. They both show the compress axes at near horizontal planes, while the tension axes are more diffused from near vertical to horizontal. This suggests that the mechanisms of the earthquake sequence are combinations of thrust and strike-slip mechanisms.

To identify the possible fault plane of the Chiali earthquake, we make a profile (AA') perpendicular to the strike of the earthquake sequence as shown in Figure 8 for the earthquakes with magnitude greater than 4. Although the locations of the offshore earthquake sequence might not be very reliable, the locations here can still provide us information about the trend of the earthquake distribution. The events in profile AA' shows a northwest dipping plane. The distribution of the earthquake sequence with strike in the northeast-southwest direction and dip in the northwest direction is comparable with one of the fault planes of the

Table 3. The optimum first-motion mechanism and the waveform mechanism of the earthquake sequence. The estimated seismic moment and the stations used in the waveform analysis are also listed.

Event number	First-motion mechanism (deg.)			Waveform mechanism (deg.)			Seismic moment (dyne-cm)	Station used
	Strike	Dip	Rake	Stirke	Dip	Rake		
E-0	160	50	80	-19	29	44	5.18×10^{24}	BCH, KLI
E-1	160	40	50	-177	41	78	8.90×10^{22}	SHK, KLI
E-2	-50	90	50	-147	39	-164	2.13×10^{22}	DAH, CHI
E-3	0	70	110	167	69	142	2.40×10^{22}	CHI, BAI
E-4	70	50	-10	-127	48	138	9.54×10^{24}	KLI, BAI
E-5	170	40	150	-8	46	70	1.38×10^{24}	KLI, BAI
E-6	170	40	130	-162	49	134	6.64×10^{22}	KLI, BAI, CHI

Optimum First-Motion Mechanisms
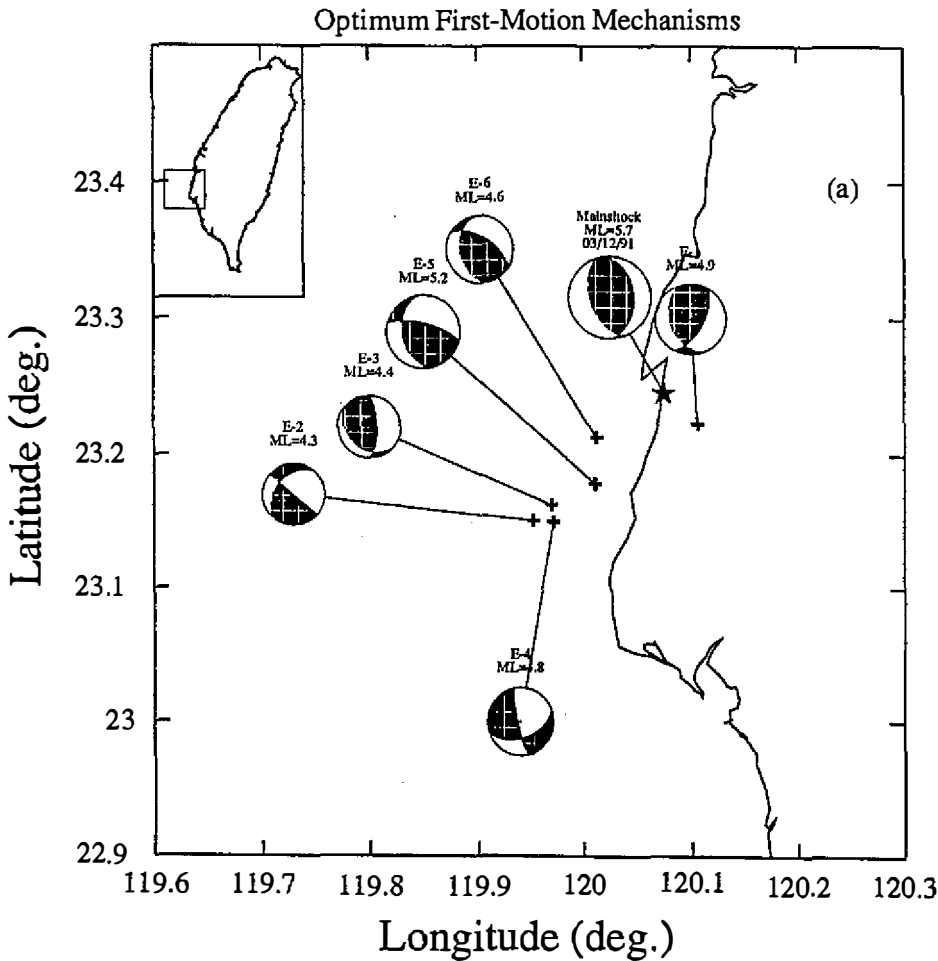
Fig. 6. Spatial distribution of the mainshock and the aftershocks of the Chiali earthquake sequence, with focal mechanisms, (a) for optimum first-motion mechanism (b) for the waveform mechanism, shown by equal-area projection of the lower focal hemisphere. The asterisks indicate the location of the mainshock. Cross symbol represent the locations of the events. The dimension of the focal sphere is proportional to the size of the earthquake.

waveform mechanisms for most earthquakes, except for event E-3 to the south of the earthquake sequence. However, the optimum first motion mechanisms show more complex focal mechanisms with more strike-slip motion components compared with the waveform mechanisms. On the basis of the waveform mechanisms, we suspect that the occurrence of the earthquake sequence might be associated with the NE-SW striking and NW dipping plane.

The focal mechanisms of the earthquake sequence from first motion data and waveform data show most of thrust faulting mechanisms with some strike-slip component. The offshore

Waveform Mechanisms
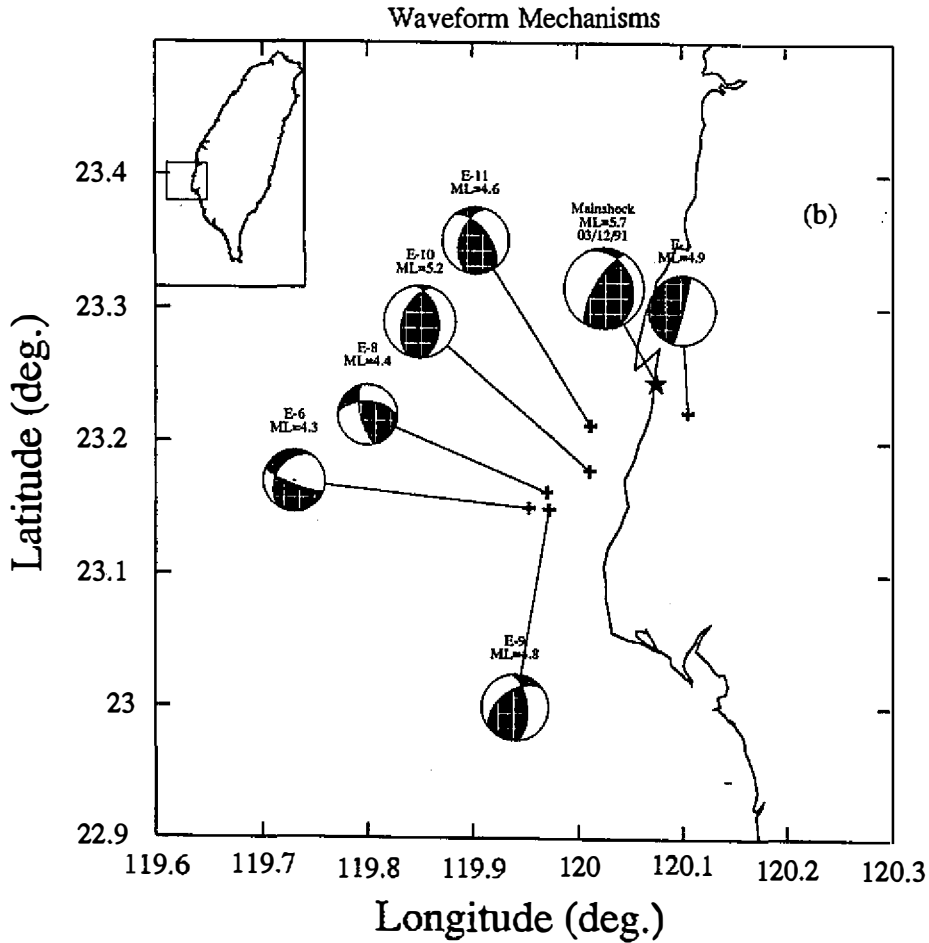
(*Fig. 6.* continued)

bathymetry data made and compiled by Liu et al. (1997) delineate some normal faults in the southwestern offshore region of Taiwan. These thrust faulting mechanisms seem to contradict their observations. Since the Chiali earthquake occurred at the depth of about 12 km without the observed surface ruptures, it is difficult to relate the earthquake directly to known surface active faults in that region. The geological tectonic setting in this region (Hsu and Sibuet, 1995) shows that the Chiali earthquake occurred in the western margin of the onshore Tainan basin. Also, the location of the earthquake is near the transition between the extension mechanism of southwestern Asian passive margin and the compression mechanism due to Luzon arc collision as shown in Figure 9 (Hsu, personal communication, 1999). The margin of the Tainan basin can be treated as weak zones, which were responsible for the occurrence of the earthquake. The thrust faulting mechanism of the Chiali earthquake might indicate an on-going compression mechanism due to the arc-continental collision in such an extensional environ-

a.

b.

P,T axes

P,T axes

*determine by
first motion*

*determine by
waveform inversion*
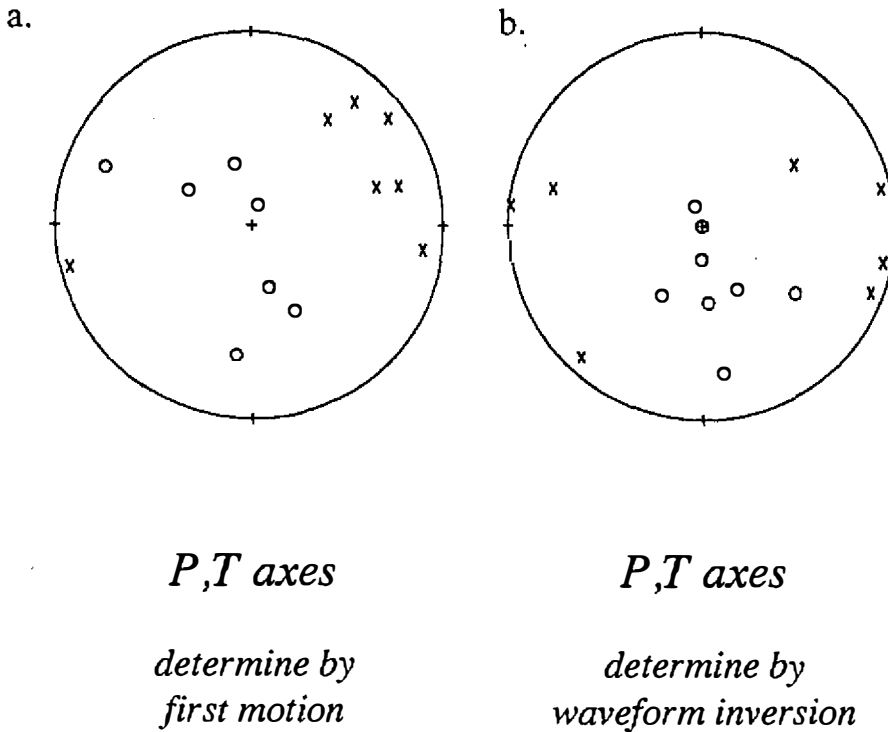
Fig. 7. The distribution of P and T axes of the earthquake sequence. (a) for the optimum first-motion mechanism, (b) for the waveform mechanism.

ment. The eastern onshore Tainan basin had been well recognized as a compression environment, where an active thrust fault as Chuko fault had been well identified. Our results on this earthquake suggest that the western margin of the onshore Tainan basin is undergoing a transition from extension to compression.

The b value of Gutenberg-Richter's magnitude-frequency relation (Gutenberg and Richter, 1955) is thought to be closely related to tectonic characteristics (Miyamura, 1962, 1969; Mogi, 1962, 1967; Bath, 1981; Hatzidimitriou et al., 1985). The b value of 0.7 as shown in Figure 10 was obtained using the earthquakes in the present study region with focal depths of less than 35 km during 1973 to 1994. Wang (1988) divided the Taiwan region into a number of 20' x 20' blocks and calculated the b value for each block for shallow events during 1973 to 1984. He obtained the b values in Taiwan region are between 0.6~2.05. The relative small b value in the study region suggests the stable tectonic environment of this region compared with other regions in Taiwan.

Ma and Kanamori (1991) calculated the ratio of the logarithm of cumulative seismic moment of aftershocks to that of the seismic moment of the mainshock for the 1988 Pasadena, California earthquake. This ratio can reflect the energy release during the mainshock and the aftershocks. In addition to the Chiali earthquake, we calculated the ratio of the cumulative

1991/3/1~3/31 Earthquakes in Chiali
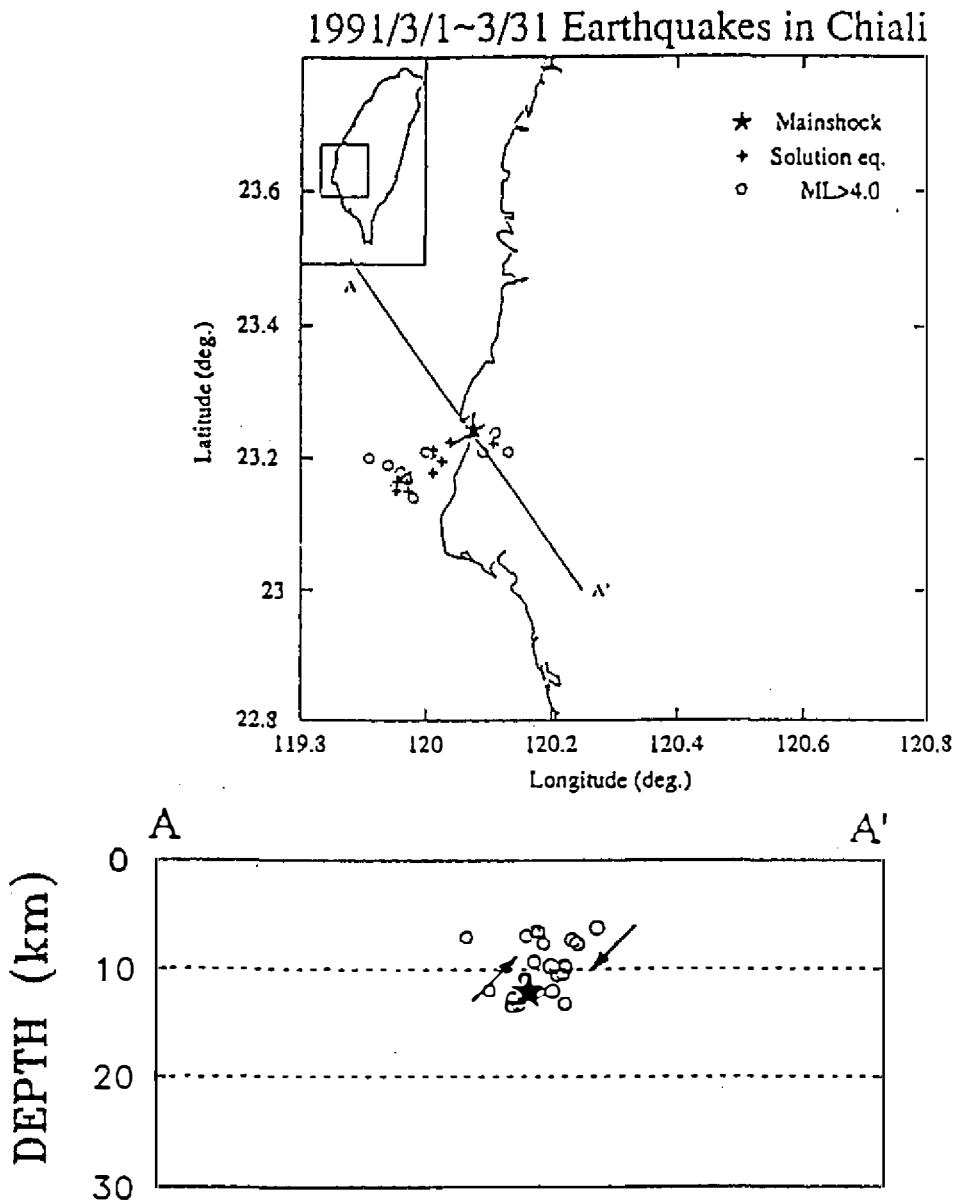
Fig. 8. The spatial distribution of the aftershock sequence with magnitude greater than 4.0 (open circles) and the profile AA' perpendicular to the strike of the aftershock distribution. The bottom figure shows the projection of the aftershock sequence along the profile AA'. The arrows indicate the possible motion of the fault. The asterisk indicates the location of the mainshock. The cross symbol indicates the earthquakes used in this study.

seismic moments of aftershocks to that of the seismic moment of mainshock for earthquakes with magnitudes greater than 5.5 in the Chainan plain region since 1973 for comparison. Except for the Chiali earthquake sequence, the seismic moments of the aftershocks and mainshock were estimated through the empirical seismic moment - magnitude relation developed by Chiang (1994). The seismic moments of the Chiali earthquake sequence are obtained through the waveform inversion analysis (also listed in Table 2). For the aftershocks whose waveform mechanisms are not available, the empirical seismic moment - magnitude relation is applied to obtain its seismic moment.

Figure 11 shows the comparison of the ratio of the logarithm of cumulative seismic moment of aftershocks to that of the seismic moment of the mainshock for the Chiali earthquake sequence to other five events in Chainan region. Most of the events have ratios between 0.1 to 0.01. The Chiali earthquake sequence, with the ratio of about 1, shows larger ratio than other sequences, indicating smaller stress drop of the Chiali earthquake compared to other earthquakes in the Chainan region.

6. CONCLUSIONS

By considering the waveform mechanism, determined by considering the amplitude ratios of P, SV and SH waveform as the constraint, we chose the optimum first-motion mechanisms among the multiple first-motion solutions of the earthquake sequence. Either the optimum first-motion mechanisms or the waveform mechanisms of most of the aftershocks show thrust faulting mechanism. Except for event E-3, the waveform mechanisms of the earthquake sequence have a northeast-southwest striking plane similar to the distribution of aftershock sequence, while the optimum first-motion mechanisms of the earthquake sequence do not delineate a consistent striking plane similar to the distribution of the aftershock. Compared with the aftershock distribution, considering the waveform mechanisms of the earthquake sequence, the fault plane with NE-SW strike and NW dipping plane is considered the preferred fault plane. The thrust faulting mechanism of the Chiali earthquake might indicate an ongoing compression mechanism due to arc-continental collision in an extensional environment as southwestern Asian passive margin. Our results on this earthquake also suggest that the western margin of the onshore Tainan basin is undergoing a transition from extension to compression. The b value of about 0.7 in this region implies a relatively stable tectonic environment compared to other regions in Taiwan. The larger ratio of the logarithm of cumulative seismic moment of aftershocks to that of the seismic moment of the mainshock for the 1991 Chiali earthquake (about 1) also suggests the smaller stress drop of the earthquake compared to other moderate sized earthquakes in the Chainan region.
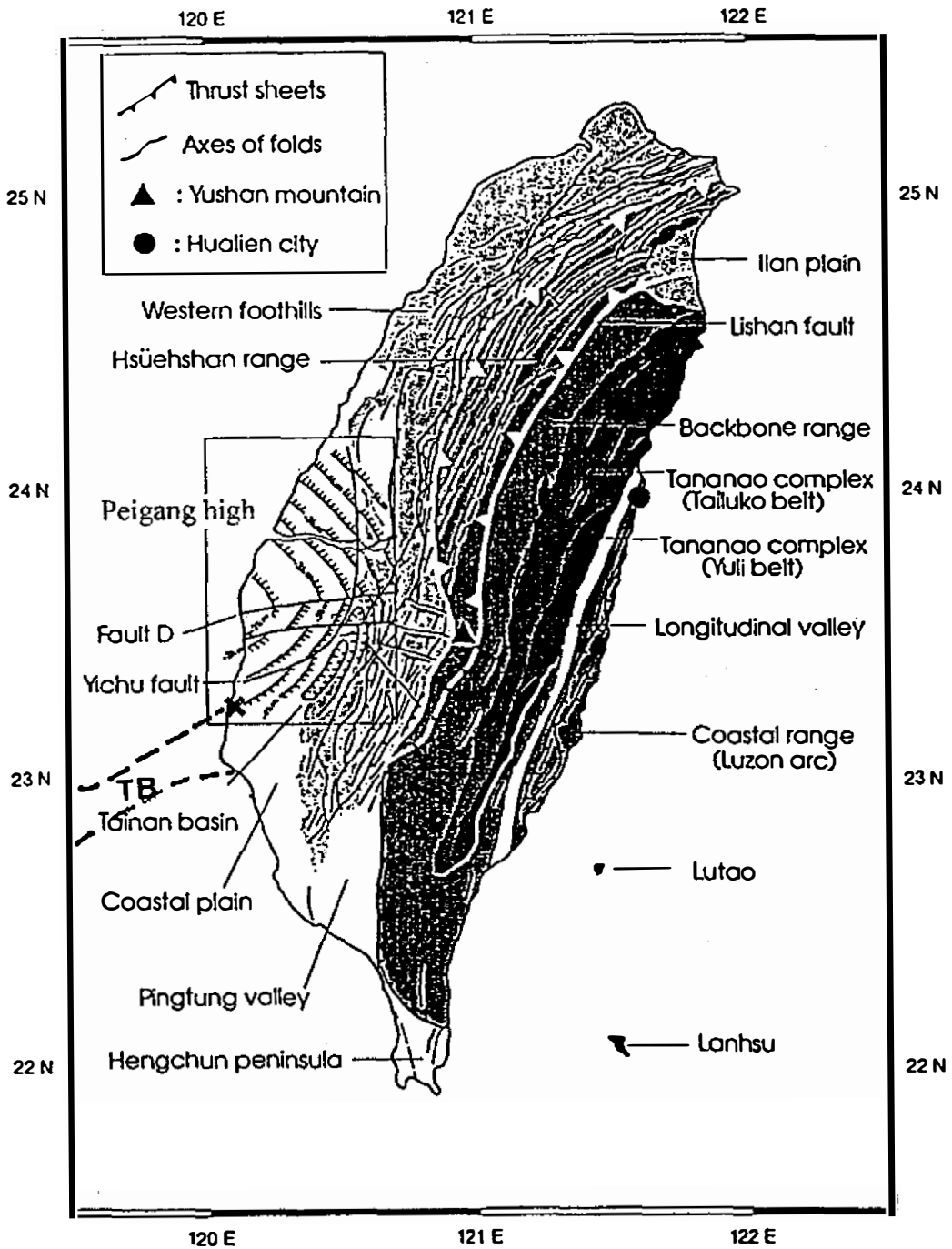
Fig. 9. General structure map of Taiwan adopted from Hsu and Sibuet (1995). The asterisk indicates the location of the mainshock.
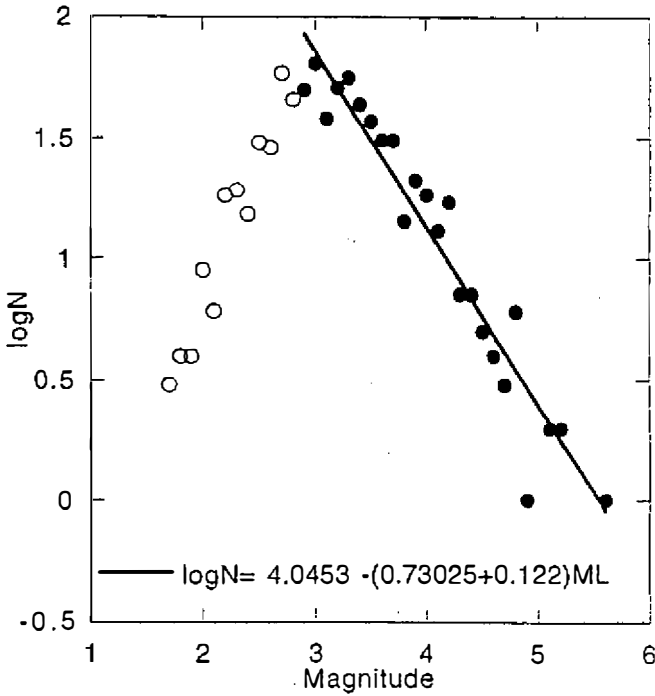
Fig. 10. Gutenberg-Richter relation of Chiali earthquake region. The solid circles are the portions used for the least-square regression of b-value, while the open circles are not included in the regression. The solid line indicates the regression result with b vale of about 0.73.
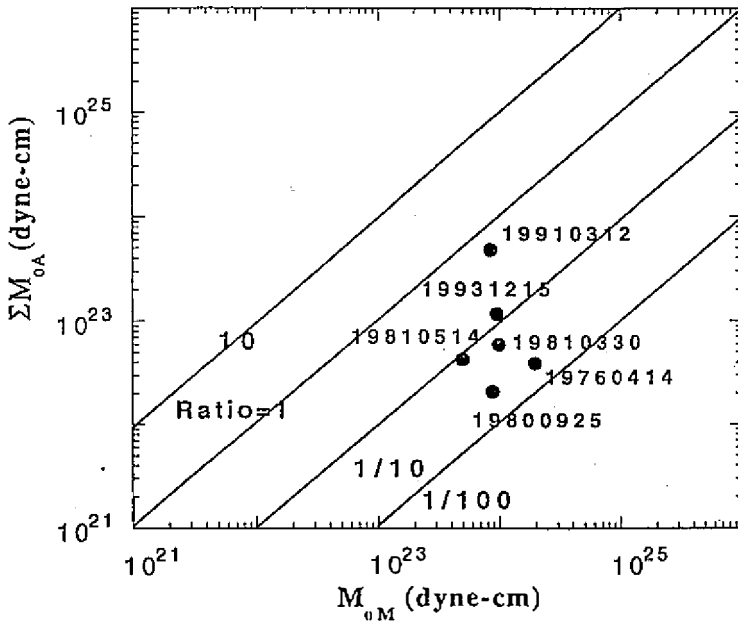
Fig. 11. The ratio of the logarithm of cumulative seismic moments of aftershocks to that of mainshock for the earthquakes with magnitude greater than 5.5 since 1973 in Chainan region. The solid lines indicate the ratios of 10, 1, 0.1, and 0.01, respectively. The numbers close to the solid circles indicate the earthquakes with year-month-date.

REFERENCES

Bath, M., 1981: Earthquake magnitude-Recent research and current trend, *Earth Sci. Rev.* 17, 315-398.

Chiang, C. H., 1994: Source scaling model in Tawain area, National Central Univ., master thesis, 77pp.

Gutenberg, B. and C. F. Richter, 1955: Frequency of earthquakes in California, *Bull. Seism. Soc. Am.*, **34**, 185-188.

Hatzidimitriou, P. M., E. E. Papadimitriou, D. M. Mountrakis, and B. C. Papazachos, 1985: The seismic parameter b of the frequency-magnitude relation and its association with the geological zones in the area of Greece, *Tectonophysics*, **120**, 141-151.

Hsu, L.W. and M. Y. Ho, 1993: The temperal and spatial distribution of the aftershocks in Taiwan region, CWBSN project report, 1~8.

Hsu, S.-K. and J. C. Sibuet, 1995: Is Taiwan the result of arc-continent or arc-arc collision?, Earth and Planet. Sci. Lett., 136, 315-324.

Ho, M. Y., 1994: Three dimensional velocity structure of western Taiwan, National Central Univ. master thesis, 108pp.

Liu, C. S., I. L. Huang, and L. S. Teng, 1997: Structure features off southwestern Taiwan, *Mar. Geol.*, 137, 305-319.

Ma, K. F. and H. Kanamori, 1994: Broadband waveform obervation of the 28 June 1991 Sierra Madre Earthquake sequence (ML=5.8), *Bull. Seism. Soc. Am.*, 84, 1725-1738.

Miyamura, S., 1962: Magnitude-frequency relation of eartqhuakes and its bearing in geotectonics, *Proc. Japan Academy*, **38**, 27-30.

Miyamura, S., 1969: The seismicity of Japan and the surrounding area (translated by Buchner), *Izv. Earth Phys.*, **7**, 21-50.

Ma, K.F. and H. Kanamori, 1991: Aftershock sequence of the 3 December 1988 Pasadena earthquake, *Bull. Seism. Soc. Am.*, **81**, 2310-2319.

Mogi, K., 1962: Study of elastic shocks caused by the fracture of heterogeneous materials and its relations to eartqhuake phenomena, *Bull. Earthquake Res. Inst.*, *Tokyo Univ.*, **40**, 125-173.

Mogi, K., 1967: Regional variations in magnitude-frequency relation of eartqhuakes, *Bull. Earthquake Res. Inst.*, *Tokyo Univ.*, **5**, 67-86.

Reasenberg, P. and D. Oppenheimer, 1985: FPFIT, FPPLOT, and FPPAGE: Fortran computer programs for calculating and displaying eartqhuake fault-plane solutions, *U.S. Geol. Surv. Open-File Rept.*, 85-739.

Shin, T.C., 1995: Application of waveform modeling to determine focal mechanisms of the 1993 Tapu earthquake and its aftershocks, *TAO*, 6, 167-180.

Tsai, Y. B. and J. M. Chiu, 1976: An active fault at the estuary of the Tsengwen-hsi in southwestern Taiwan, *Petro. Geology of Taiwan*, 209-224.

Wang, J. H., 1988: b values of shallow earthquakes in Taiwan, *Bull. Seism. Soc. Am.*, **78**, 1243-1254.